

Federated Continual 3D Segmentation With Single-round Communication

Can Peng^a, Qianhui Men^{a,b}, Pramit Saha^a, Qianye Yang^a, Cheng Ouyang^a, J. Alison Noble^a

^aUniversity of Oxford, Oxford, United Kingdom

^bUniversity of Bristol, Bristol, United Kingdom

Abstract

Federated learning seeks to foster collaboration among distributed clients while preserving the privacy of their local data. Traditionally, federated learning methods assume a fixed setting in which client data and learning objectives remain constant. However, in real-world scenarios, new clients may join, and existing clients may expand the segmentation label set as task requirements evolve. In such a dynamic federated analysis setup, the conventional federated communication strategy of model aggregation per communication round is suboptimal. As new clients join, this strategy requires retraining, linearly increasing communication and computation overhead. It also imposes requirements for synchronized communication, which is difficult to achieve among distributed clients. In this paper, we propose a federated continual learning strategy that employs a one-time model aggregation at the server through multi-model distillation. This approach builds and updates the global model while eliminating the need for frequent server communication. When integrating new data streams or onboarding new clients, this approach efficiently reuses previous client models, avoiding the need to retrain the global model across the entire federation. By minimizing communication load and bypassing the need to put unchanged clients online, our approach relaxes synchronization requirements among clients, providing an efficient and scalable analysis framework suited for real-world applications. Using multi-class 3D abdominal CT segmentation as an application task, we demonstrate the effectiveness of the proposed approach.

Keywords: Federated Continual Learning, Multi-class Segmentation

1. Introduction

Federated Learning (FL) is an attractive analysis framework for sensitive data areas such as healthcare imaging where real-world data cannot be shared for legal and privacy reasons. However, most existing approaches focus on basic classification tasks and assume a fixed FL setting, overlooking more realistic scenarios that might be met in a research collaboration or real-world use case setting where new clients may join or data distributions of existing clients will evolve as new data is collected. Figure 1 shows an example of a continually evolving FL scenario. This paper addresses FL modelling in such dynamic settings, which are both challenging and essential for real-world downstream applications and future deployment in clinical research and hospital settings.

Specifically, we address *federated continual learning* (FCL) in the context of multi-class 3D segmentation, both under-explored topics compared to fixed FL and to FL-based classification, respectively. Although FL has rapidly evolved, the client-server communication strategy introduced by the classic FedAvg method (McMahan et al., 2017), which performs model aggregation per communication round (MAPCR), still

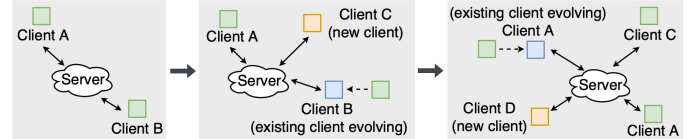


Figure 1: The pipeline for the FCL task. In an FCL setting, new clients may join the federation over time, and the data distribution of existing clients can shift as additional data becomes available locally.

dominates the design of FL methods. However, MAPCR demands frequent client-server communication, strict synchronization, and identical model architectures. In FCL settings, where new clients may join or existing ones may be updated, MAPCR can become impractical. MAPCR requires all clients to have continuous access to all their data, which is often impossible in real-world scenarios due to privacy, licensing, or data storage constraints. Even when data availability is not an issue, MAPCR requires all clients to retrain the updated global model from scratch, significantly increasing both computational and communication overhead.

To address the inherent limitations of MAPCR, we propose an alternative novel communication strategy called Multi-Model Distillation in the Server (MMDS). MMDS constructs a global model through a one-time asynchronous interaction between clients and the server. In this approach, each client first trains their model locally. The server then performs multi-model distillation to generate the global model. The proposed framework is illustrated in Figure 2. This strategy overcomes

Email addresses: can.peng@eng.ox.ac.uk (Can Peng), qianhui.men@eng.ox.ac.uk (Qianhui Men), pramit.saha@eng.ox.ac.uk (Pramit Saha), qianye.yang@eng.ox.ac.uk (Qianye Yang), cheng.ouyang@eng.ox.ac.uk (Cheng Ouyang), alison.noble@eng.ox.ac.uk (J. Alison Noble)

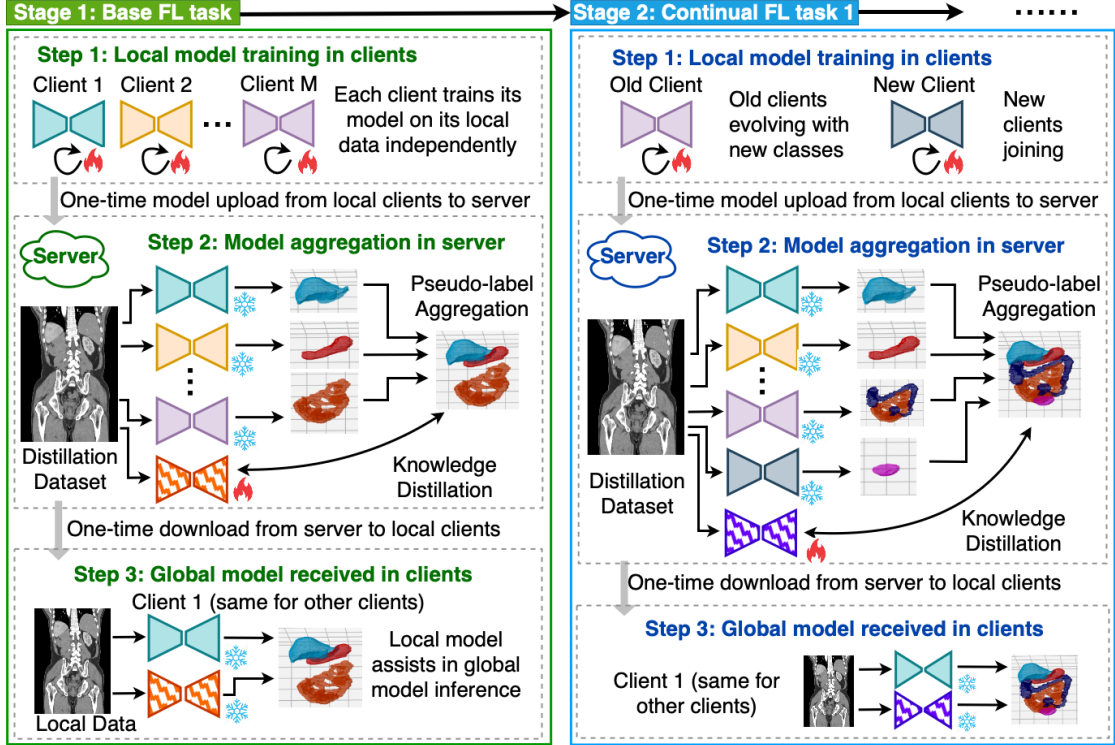


Figure 2: Proposed MMDS framework. Initially, each client trains a model locally and uploads it to the central server. The server aggregates the local models using knowledge distillation on publicly available data to produce a global model, which is redistributed to clients. Each client integrates the global model with its local model for inference, preserving its knowledge while benefiting from shared knowledge. When new clients join or existing clients evolve, the new or revised local models are uploaded to the server. The server then performs distillation again to incorporate the new contributions into the global model, with the updated global model redistributed to all clients. This process is repeated when updates occur on the client side.

the rigidity of MAPCR, offering a flexible and efficient solution for FCL while presenting a fresh perspective on the FL communication strategy. The key contributions of this paper are:

- We present a flexible framework for FCL that supports new client joining and efficient analysis of evolving client data distributions.
- We analyze the standard FL communication strategy and based on its strengths and limitations, propose a novel communication strategy for FCL.
- To place the contribution in context, we validate our approach on six publicly available 3D abdominal CT segmentation datasets comprising 19 abdominal organs and associated pathological structures under various FL protocols, demonstrating its advantages over prior work.

2. Related Work

2.1. Federated Continual Learning (FCL)

Most current FL frameworks consider a fixed setting with constant training objectives. This traditional FL framework primarily addresses non-IID static data with spatial heterogeneity. Recently, researchers have begun to explore temporal heterogeneity by introducing continual learning within FL (Usmanova et al., 2021; Dong et al., 2022; Ma et al., 2022; Qi et al., 2023; Tran et al., 2024; Babakniya et al., 2024; Zhang et al., 2023; Li et al., 2024). In FCL, the federation updates the global model to adapt to changing client needs. For instance, new clients

may join, and existing clients may modify the model to accommodate changes in their objects of interest. Some approaches tackle this challenge using synthetic data replay (Dong et al., 2022; Qi et al., 2023; Tran et al., 2024; Babakniya et al., 2024; Zhang et al., 2023), while others employ memory replay, selectively retaining representative old data locally (Usmanova et al., 2021; Li et al., 2024). In terms of application tasks, most current FCL research has focused on image classification. To the best of our knowledge, our work is the first to investigate FCL in the context of multi-class 3D segmentation.

2.2. Federated Medical Image Segmentation

Current literature addresses various aspects of federated medical image segmentation; distribution shift (Liu et al., 2021; Xu et al., 2022; Wang et al., 2022, 2023), weak annotations (Zhu et al., 2023; Wicaksana et al., 2022), and noisy labels (Wu et al., 2024). Most studies focus on binary segmentation, while multi-class segmentation remains relatively under-explored, despite its practical importance. This paper considers federated multi-class segmentation for 3D abdominal CT scans. For this task, Xu et al. proposed class-specific encoders to improve feature extraction (Xu et al., 2023). Kim et al. used knowledge distillation for regularization (Kim et al., 2024). As summarized in Table 1, both methods rely on frequent client-server communication and are limited to fixed FL scenarios. In contrast, our approach is designed for FCL scenarios and requires only one-time model aggregation to generate the global model.

Task	Challenge	Exchanged information		MAPCR	KD approach	
		Sent	received		Client-side	Server-side
FAug (Jeong et al., 2018)	Cl	NIID, CE	\bar{z}	\bar{z} + generator	✓	regularizer + generator
FedDF (Lin et al., 2020)	Cl	NIID, MH	ω	ω	✓	- digestion + D_p
CFD (Sattler et al., 2021)	Cl	MH, CE	\tilde{y}_p	\tilde{y}_p	✓	digestion + D_p digestion + D_p
FedAD (Gong et al., 2021)	Cl	MH, CE	z_p, A_p	-	✗	- digestion + D_p
FedGKT (He et al., 2020)	Cl	MH, CE	z, H, y	z	✓	regularizer regularizer
Chen et al. (Chen et al., 2023)	Cl	P	ω	ω	✓	regularizer -
Target (Zhang et al., 2023)	Cl	CL	ω	$\omega + D_s$	✓	regularizer generator
Re-Fed (Li et al., 2024)	Cl	CL	ω	ω	✓	- -
CFeD (Ma et al., 2022)	Cl	NIID, CL	ω	ω	✓	digestion + D_p digestion + D_p
Fed-MENU (Xu et al., 2023)	Seg	NIID	ω	ω	✓	- -
Kim et al. (Kim et al., 2024)	Seg	NIID	ω	ω	✓	regularizer -
Ours	Seg	NIID, P, CE, MH, CL	ω	ω	✗	- digestion + D_p

Table 1: Comparison of related FL methods with ours. FL challenges addressed: data non-iidness (NIID), model heterogeneity (MH), communication efficiency (CE), personalization (P), and continual learning (CL). Symbols: ω model parameters, z logit vectors (model output before softmax), \bar{z} class-wise average logit vectors, y labels of local data, \tilde{y}_p soft targets (model output after softmax) on public data, H intermediate feature maps, A attention maps, D_p extra public data, D_s synthetic data. Regularizer: uses KD to regularize training. Digestion: uses KD to supervise training.

2.3. Knowledge Distillation (KD) in FL

KD (Hinton, 2015) has been widely adopted in FL due to its ability to transfer knowledge without requiring access to the original training data. For example, KD can be used to improve communication efficiency (CE) (Jeong et al., 2018), to alleviate model heterogeneity (MH) (Lin et al., 2020; Afonin and Karimireddy, 2021) and to support personalization (P) (Chen et al., 2023). Additionally, KD has been applied to mitigate forgetting in FCL (Ma et al., 2022; Zhang et al., 2023; Li et al., 2024). Table 1 compares our approach with representative, and closely related KD-based FL methods¹. Existing methods often address only one or two specific FL challenges, such as CE, MH, P, or FCL. However, in real-world FL scenarios, these challenges are often interconnected, which requires a unified solution to address them simultaneously. Furthermore, most methods rely on the MAPCR strategy, which requires frequent client-server communication. We argue that the frequent communication of MAPCR imposes limitations in tackling challenges such as communication synchronization and FCL. To address these interconnected challenges, we propose a novel framework that does not use MAPCR while offering a unified solution to challenges such as CE, MH, P, and FCL.

3. Problem Formulation

The FCL multi-class 3D segmentation task consists of T stages. In stage 1, a set of \mathcal{M}_1 clients predict a set of C_1 classes. In each subsequent stage t , \mathcal{M}_t clients join or expand the number of their predictive targets, introducing C_t new classes into the federated system. At each stage t , the objective is to train a global segmentation model that can effectively segment across the combined label set ($\bigcup_{i=1, \dots, t} C_i$) for all clients ($\bigcup_{i=1, \dots, t} \mathcal{M}_i$), while ensuring that no data is shared between clients or with the

Algorithm 1 Multi-Model Distillation in the Server (MMDS)

Input: T : continual FL stages; \mathcal{M}_t : clients updated or added at stage t ; S_t : total clients by stage t ; \mathcal{D}_k : local dataset of client k ; \mathcal{D}_{dist} : server distillation dataset; w : model parameters; w_0 : randomly initialized model parameters.

```

1: for  $t = 1$  to  $T$  do                                 $\triangleright t$ -th stage continual FL
2:   // Step 1
3:   for each client  $k \in \mathcal{M}_t$  in client parallel do     $\triangleright$  Local model training
4:      $w_t^k \leftarrow \text{ModelTrain}(\mathcal{D}_k, w_0^k)$ 
5:     Send the completely trained client model  $w_t^k$  to the server.
6:   end for
7:   // Step 2
8:   In server, update stored old models with received ones correspondingly.
9:   for each client model  $k \in S_t$  in server do     $\triangleright$  Generate pseudo-label
10:     $\hat{y}^k \leftarrow \text{ModelInference}(\mathcal{D}_{dist}, w_t^k)$ 
11:   end for
12:    $\tilde{y} \leftarrow \text{PredictionAggregation}(\hat{y}^1, \hat{y}^2, \dots, \hat{y}^{|S_t|})$            $\triangleright$  Equation 1
13:    $w_t^G \leftarrow \text{MultiModelDistillation}(\mathcal{D}_{dist}, \tilde{y}, w_0^G)$            $\triangleright$  Equations 2, 3, 4
14:   // Step 3
15:   Distributes global model  $w_t^G$  to all clients.
16: end for

```

central server. Clients may specialize in different anatomy targets, such as the kidney: {kidney, kidney stone, kidney tumor} or the liver: {liver, liver tumor}, which can result in missing or mismatched annotations. Additionally, some clients may have overlapping segmentation targets due to shared interest in certain anatomical targets.

4. Methodology

The complete framework of the proposed method is illustrated in Figure 2, with the corresponding pipeline detailed in Algorithm 1. Our method, Multi-Model Distillation in the Server (MMDS), eliminates the need for frequent and synchronized communications between clients and the server by allowing clients to train their local models independently. After completion of local training, clients upload their fully trained models to the server. The server aggregates the client models using

¹For a survey covering a broader scope, refer to Mora et al. (2024).

	m clients (initial session) →		+ n new clients →		+ k new clients →	
communication load on the server						
	# participated clients	# communication	# participated clients	# communication	# participated clients	# communication
MAPCR	m	$2mE$	$m + n$	$2(m + n)E$	$m + n + k$	$2(m + n + k)E$
computation usage of the federation						
	offline training	# computation	offline training	# computation	offline training	# computation
MAPCR	✗	mO	✗	$(m + n)O$	✗	$(m + n + k)O$
MMDS	✓	$(m + 1 + \epsilon)O$	✓	$(n + 1 + \epsilon)O$	✓	$(k + 1 + \epsilon)O$

Table 2: Comparison of communication and computation load for different communication strategies in FCL: classic MAPCR vs proposed MMDS. Each server data transmission is counted as one communication. E denotes the total communication rounds needed for convergence in MAPCR, $E \gg 1$. O denotes model training computation per client model (assumed to be similar across client models). $\epsilon \ll 1$ indicates the minimal inference cost for generating distillation pseudo-labels on the server.

multi-model distillation on publicly available unlabeled data to generate the global model. This global model is then distributed back to each client, allowing them to integrate it with their local model. When new clients join or existing clients update their models with new data, the new or revised local models are uploaded to the server. The server, which stores all previous client models, adds the new one (if from the new client) or replaces outdated client models with updated ones (if from the updated existing client) while retaining models from clients without new updates. It then performs distillation again to incorporate the new contributions into the global model, with the updated global model redistributed to all clients. This process is repeated when updates occur on the client side. Through continuous aggregation, the FL system efficiently accommodates new clients and ensures that all participants are updated with the latest global model.

4.1. Local Model Training

In our framework, each client first trains its model locally using annotated data through a standard supervised learning pipeline. Since clients may annotate images for different purposes, they often focus on different segmentation targets, leading to variations in the number of prediction classes and class overlaps across clients. To accommodate mismatched label space across clients, we employ CLIP-DrivenSeg (Liu et al., 2023) as our backbone. This network leverages CLIP embeddings (Radford et al., 2021) to represent each class, allowing the network to dynamically extend its prediction classes without structural modifications. During local supervised training, as annotations are limited to a subset of target classes relevant to each client, binary cross-entropy loss and binary dice loss are used. These losses are computed and back-propagated exclusively for the classes with corresponding annotations, ensuring that precise supervision is applied only to the labeled classes.

4.2. Server Distillation

After local training, client models are sent to the server for aggregation. On the server side, knowledge distillation (KD) (Hinton, 2015) is utilized for model aggregation, using a publicly available unlabeled dataset as the distillation dataset.

Pseudo-labels for the distillation dataset are generated based on predictions from the client models. Each client runs a one-time inference on the distillation dataset to produce its predictions, which are then aggregated to create the pseudo-labels. Given that clients may have overlapping segmentation targets, an effective pseudo-label aggregation strategy is required. For classes with predictions from multiple models, entropy impurity (Shen et al., 2019) is used to quantify prediction ambiguity. For each distillation sample, the prediction with the lowest entropy impurity, indicating the highest confidence, is selected as the pseudo-label for that class. The entropy impurity for class c for a given input image is calculated as follows:

$$\mathcal{I}_c = - \sum_{n=1}^N \hat{y}_{c,n} \log(\hat{y}_{c,n}) \quad (1)$$

where $\hat{y}_{c,n}$ denotes the predicted probability for the n -th pixel in the c -th class segmentation mask. N is the total number of pixels in the segmentation mask.

Global model training adopts the same strategy as local model training, utilizing both soft binary cross-entropy loss and soft Dice loss. These loss functions are defined as follows:

$$\mathcal{L}_{\text{CE}} = -\frac{1}{C} \sum_{c \in \bigcup_{i=1, \dots, t} C_i} \frac{1}{N} \sum_{n=1}^N [\tilde{y}_{c,n} \log(\hat{y}_{c,n}) + (1 - \tilde{y}_{c,n}) \log(1 - \hat{y}_{c,n})] \quad (2)$$

$$\mathcal{L}_{\text{DICE}} = \frac{1}{C} \sum_{c \in \bigcup_{i=1, \dots, t} C_i} \left[1 - \frac{2 \sum_{n=1}^N \hat{y}_{c,n} \tilde{y}_{c,n}}{\sum_{n=1}^N \hat{y}_{c,n}^2 + \sum_{n=1}^N \tilde{y}_{c,n}^2} \right], \quad (3)$$

$$\mathcal{L}_{\text{dist}} = \mathcal{L}_{\text{CE}} + \mathcal{L}_{\text{DICE}} \quad (4)$$

where $\tilde{y}_{c,n}$ denotes the aggregated pseudo-label derived from the client models. $\bigcup_{i=1, \dots, t} C_i$ represents the set of classes included in the t th FCL stage.

4.3. Communication and Computation Complexity Analysis

As shown in Table 2, the proposed MMDS strategy offers several advantages over the commonly used MAPCR approach: 1) By performing a one-time aggregation after full local training, MMDS largely reduces communication costs and eliminates the need for strict synchronization between clients and

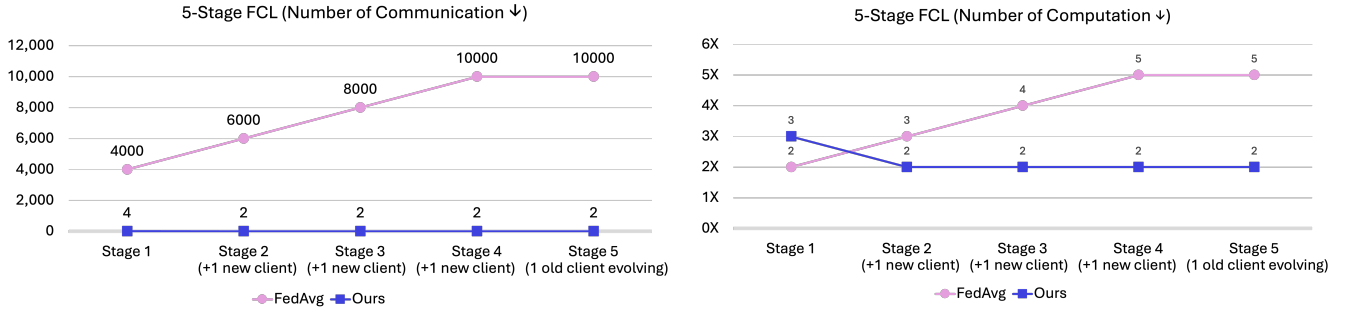


Figure 3: Comparison of communication and computation loads between the classic MAPCR-type method FedAvg and the proposed method during 5-stage FCL segmentation across five clients. Here 1X represents the computation required to train a single model to convergence (assumed to be similar across client models).

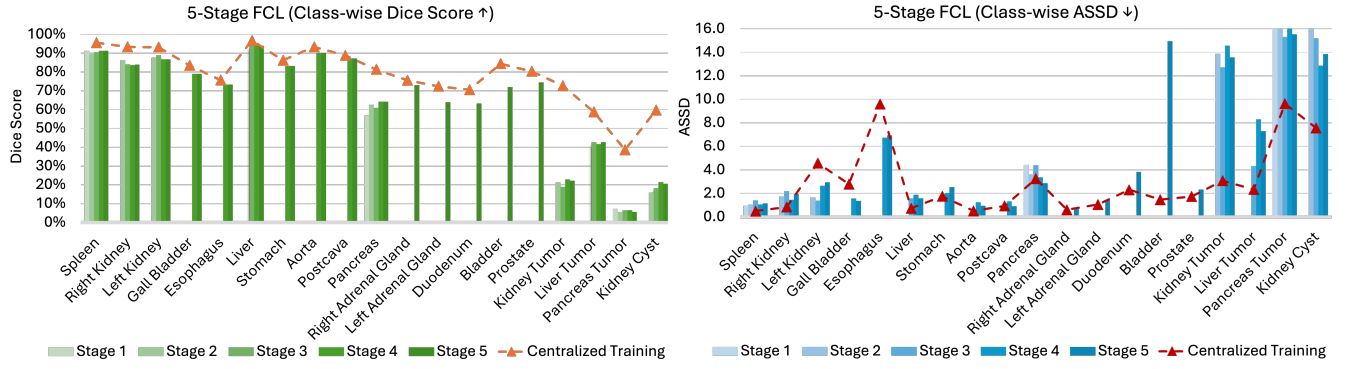


Figure 4: Class-wise DICE score and ASSD performance of the proposed method on 5-stage FCL segmentation across five clients.

the server. 2) In FCL scenarios, MAPCR requires all clients to jointly train to update the global model while MMDS can seamlessly incorporate updates. It reuses previous client models and eliminates the need for online training. 3) The computation overhead of MAPCR is proportional to the total number of clients. As the client base grows in FCL scenarios, the overhead of MAPCR scales linearly. In contrast, MMDS maintains significantly lower costs, as its overhead depends only on the number of new clients. 4) MMDS uses KD to derive the global model to mimic client models’ input-output mappings, supporting diverse client model architectures.

5. Experiment

5.1. Dataset

We performed experiments with six publicly available 3D abdominal CT segmentation datasets, encompassing annotations for 19 abdominal organs and associated pathologies. These datasets are: 1) LiTS dataset (Bilic et al., 2023); 2) KiTS dataset (Heller et al., 2019); 3) MSD pancreas dataset (Antonelli et al., 2022); 4) MSD spleen dataset (Antonelli et al., 2022); 5) AMOS dataset (Ji et al., 2022); 6) BCTV dataset (Landman et al., 2015). Additionally, the WORD dataset (Luo et al., 2021) is utilized as the distillation dataset. For the detailed information of all these datasets, please refer to supplementary material Appendix A.

5.2. Evaluation Metric

For segmentation performance evaluation, we use the DICE score to measure overall accuracy and Average Symmetric Surface Distance (ASSD) to assess boundary precision. Additionally, we analyze the communication and computation loads involved in generating the global model for the federation.

5.3. Task Setup

To replicate real-world multi-site scenarios, we treat each dataset as a distinct client and utilize all available annotations from it. This allows for overlap in objects of interest across clients, while also introducing unique, client-specific objects. As we focus on FCL in this work, clients are incrementally introduced to the federation. The process begins with two clients (stage 1): MSD-pancreas (Antonelli et al., 2022) and MSD-spleen (Antonelli et al., 2022). Subsequently, KiTS (Heller et al., 2019), LiTS (Bilic et al., 2023), and AMOS (Ji et al., 2022) are added. To simulate evolving clients, the AMOS dataset, which includes annotations for multiple organs, is divided into two sets with distinct classes. This setup establishes a five-stage FCL scenario, where each stage introduces a new client (stage 2, 3, 4) or updates an existing one (stage 5).

5.4. Implementation Details

The proposed method is implemented in PyTorch and CLIP-DrivenSeg (Liu et al., 2023) is used as the segmentation backbone. We follow its original training strategy utilizing the AdamW optimizer with a warm-up scheduler over 50 epochs. The initial learning rate is set to $4e^{-4}$, with a momentum of 0.9



Figure 5: Class-wise DICE score performance of each client before and after the 5-stage FCL. FCL allows clients to segment classes that are not labeled in their local datasets by sharing knowledge with other clients.

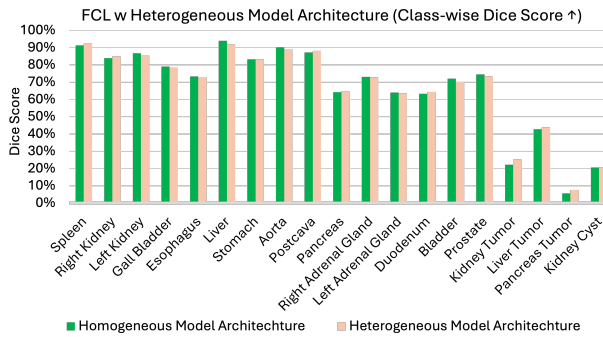


Figure 6: DICE score performance of the global model after 5-stage FCL with homogeneous and heterogeneous model architecture.

and a weight decay of $1e^{-5}$. For methods involving MAPCR, the model is trained for 1000 communication rounds, with 1 epoch per round. For methods without MAPCR, the model undergoes training for 1000 epochs.

5.5. Comparison with Benchmarks

To demonstrate the efficiency and flexibility of the proposed MMDS strategy, we compare it with the MAPCR-type method in terms of both communication and computation loads. As FedAvg is the most representative MAPCR-type method and serves as the basis for many advanced approaches with similar communication and computation loads, we compare our method with FedAvg, as shown in Figure 3. The results reveal that as the federation grows and evolves, FedAvg requires a linearly increasing communication load. For instance, after three stages of adding one new client per stage, the communication load becomes 5,000 times larger than that of the MMDS strategy. This substantial increase not only raises communication costs but also imposes strict synchronization among clients. Delays from a single client can significantly affect overall training progress. Similarly, the computation load for FedAvg doubles after three stages due to the need to retrain the global model from scratch whenever new clients join. This inflexibility arises because the MAPCR-type method relies on aggregating a global model from all participating clients. In contrast, MMDS avoids this drawback by reusing the models from clients without new updates.

Furthermore, in more data-restricted scenarios where old clients’ data cannot be accessed, MAPCR-type methods such as FedAvg become unusable. These methods require all clients’ data to be locally available for training the global model, overlooking real-world constraints, such as privacy regulations, licensing issues, or storage limitations, that may prevent access to historical data. In contrast, the MMDS strategy handles federation changes more efficiently by reusing previous client models to adaptively update the global model. This approach makes the MMDS method more practical and scalable for real-world FCL scenarios.

We also compare the segmentation performance of our proposed method with centralized training. Centralized training, which aggregates data from all clients for model development, serves as the performance upper bound. Figure 4 presents the results. After five stages of FCL, the proposed MMDS method achieves an average DICE score of 78.65% across all organ classes, compared to 85.09% for centralized training. In 12 out of 15 organ classes, MMDS achieves a DICE score greater than 70%. However, its accuracy decreases for challenging small or elongated structures like the pancreas and the duodenum. On the other hand, the performance of pathology classes, such as tumors, is notably lower. We conjecture this is because the distillation dataset, WORD (Luo et al., 2021), does not include pathology examples, limiting the activation of pathological features during distillation. Consequently, the global model lacks sufficient information to effectively learn these classes. Addressing the challenge of distilling knowledge from the teacher model without heavy reliance on distillation data remains an open question in knowledge distillation. We plan to explore this issue in future work.

5.6. Personalized FL Performance

In our approach, each client trains a local model independently before sending it to the server for aggregation. After aggregation, clients retain two models: their local model, tailored to their specific data, and the global model, which integrates knowledge from all participating clients. This dual-model structure naturally supports the personalized FL paradigm, enabling clients to maintain expertise in their local data while extending their capabilities to other domains via the global model.

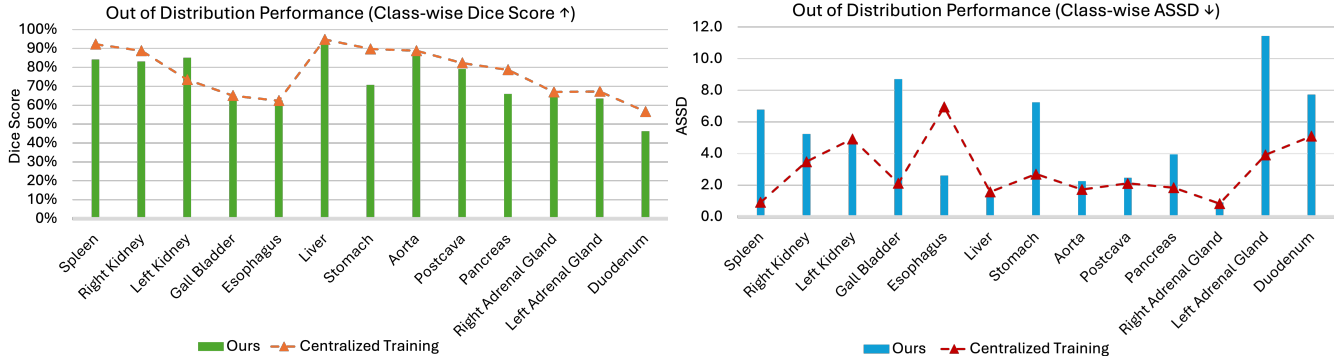


Figure 7: Out-of-distribution DICE score and ASSD performance of the global model after 5-stage FCL, evaluated on the BTCV dataset (Landman et al., 2015).

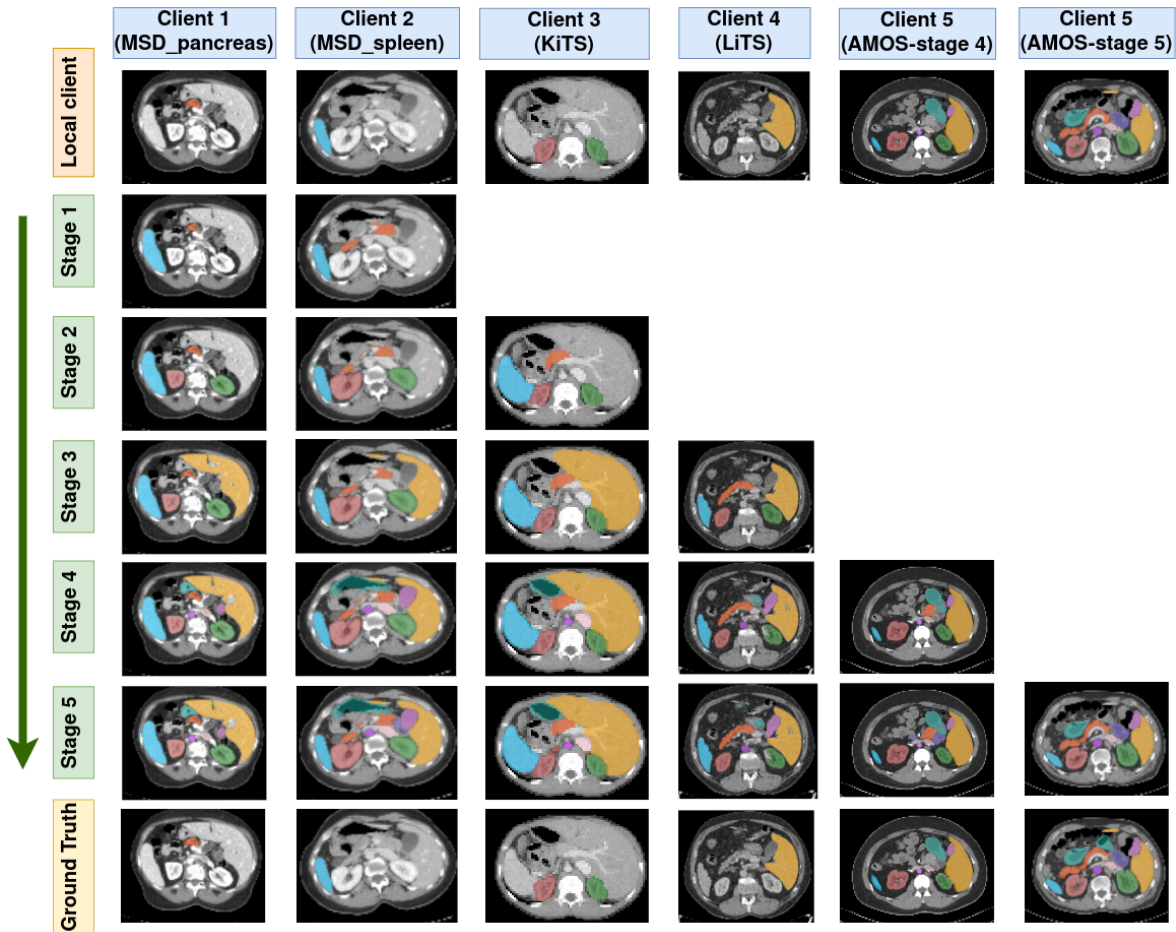


Figure 8: 2D visualizations of segmentation results produced by the proposed method under the 5-stage FCL. Each column displays a case from either a new client joining the federation or an updated client. As the federation expands and existing clients evolve, the global model progressively gains the capability to segment new objects introduced by these clients.

Personalized inference is achieved by testing samples with both the local and global models and aggregating the results. For classes where the local model is well-trained, its predictions are prioritized. Otherwise, predictions from the global model are used. Figure 5 illustrates the performance of each client before and after FCL. The results show that after FL cooperation, all clients can retain their local expertise while benefiting from the shared knowledge of the federation through the global

model.

5.7. Heterogeneous Model Architecture

Our approach supports model agnosticism in FL by allowing each client model to be independently and fully trained. The global model is then trained by aligning the input-output functions of the client models eliminating the need for homogeneous model architectures. To demonstrate the flexibility of



Figure 9: 3D visualizations of segmentation results produced by the proposed method under the 5-stage FCL.

the proposed method in handling heterogeneous model structures, we employ two types of backbones: convolutional-based and transformer-based 3D U-Nets. Specifically, Swin UNETR (Hatamizadeh et al., 2021) is used as the baseline feature extractor for the second and fourth clients, while 3D U-Net (Çiçek et al., 2016) is employed for the remaining clients. The five-step FCL process is repeated. Figure 6 presents the performance of the final global model. The results demonstrate that the proposed method effectively aggregates client models with diverse architectures, achieving performance comparable to setups where clients use homogeneous model structures.

5.8. Out-of-Distribution Performance

To assess the robustness of the proposed method, we evaluate its out-of-distribution performance using the BTCV dataset (Landman et al., 2015), which represents an external client not involved in the federation. Figure 7 presents the results. Since the "Portal Vein and Splenic Vein" class is not included in the federation (as none of the participating clients contained this

class), it is excluded from the evaluation. For comparison, the performance of the centrally trained model is provided as the upper bound. As shown in the figure, the proposed method achieves comparable performance to the upper bound on most classes, demonstrating its robustness.

5.9. Visualization

We present visualization results comparing the global model trained with our proposed method against local training and ground truth, shown in both 2D and 3D views. Figure 8 and Figure 9 display the visualization results in 2D (axial) and 3D views, respectively. Each column represents a case from a different client dataset. The middle five rows illustrate the segmentation results produced by the global model on all its client datasets after each stage of FCL learning. It can be observed that when new clients are joining or existing clients are evolving, the proposed method is flexible to adapt to the dynamic FCL scenarios and keep updating the global model to be able to segment an increasing number of objects of interest.

6. Discussion

While the proposed approach is promising, its effective implementation in real-world FCL scenarios might benefit from further consideration of certain conditions. The proposed approach relies on a distillation dataset, which underscores the need to minimize discrepancies in both semantic labels and domain gaps with client data distributions to ensure effective model distillation. In our experiments, the global model faces challenges with pathology classes, likely due to the absence of pathology examples in the distillation dataset. Learning becomes difficult for underrepresented classes in the distillation dataset. Data-free knowledge distillation for segmentation remains an open challenge, and we plan to explore this topic in future work.

Significant domain differences among different client datasets can also adversely impact the effectiveness of the distillation process. If the distillation dataset diverges considerably from the client data, its effectiveness may diminish. While in this paper, we focus on CT datasets with relatively small domain gaps between different datasets, other applications, such as MRI or ultrasound imaging, may face greater domain differences due to equipment and scanning variations. In such cases, incorporating an evaluation step prior to distillation may be necessary to ensure optimal performance. Given the distillation dataset and the client model, this evaluation step will estimate the model performance on the dataset. Exploring this aspect will also be part of our future work.

7. Conclusion

This paper concerns federated continual learning (FCL) for multi-class 3D segmentation, focusing on scenarios where new clients join and existing ones evolve. Building on an analysis of mainstream aggregation-per-round type FL methods, we propose a one-time model aggregation strategy for FCL segmentation. Our approach trains local client models independently, followed by multi-model distillation on the server. This removes frequent communication, eliminates synchronization requirements, supports heterogeneous model structures, and seamlessly incorporates updates from new or evolving clients without restarting global training. Using 3D abdominal CT segmentation as an application task, we demonstrate the effectiveness of the proposed approach across diverse FL protocols.

Acknowledgements

This work was supported by the UKRI grant EP/X040186/1 (Turing AI Fellowship). This work was also partly supported by the InnoHK-funded Hong Kong Centre for Cerebro-cardiovascular Health Engineering (COCHE) Project 2.1 (Cardiovascular risks in early life and fetal echocardiography). PS is supported by the UK EPSRC (Engineering and Physical Research Council) Programme Grant EP/T028572/1 (VisualAI), a UK EPSRC Doctoral Training Partnership award.

Appendix A. Dataset

In this section, we introduce the 3D abdominal CT segmentation datasets used in our experiments. Since different datasets provide annotations for varying classes, with some overlap between them, we followed the approach outlined in [Liu et al. \(2023\)](#) to unify the label indices across all datasets. Overall, we focus on segmenting 19 abdominal organs and pathological structures. As many datasets do not provide ground truth annotations for their test data, following [Liu et al. \(2023\)](#), we reorganize the available training sets, splitting them into training, validation, and testing subsets. The detailed information for each dataset is provided below, and a summary is presented in Table [A.3](#), including the number of training samples, the number of class labels, and the label lists.

BTCV ([Landman et al., 2015](#)) comprises 30 scans with volume size range from $[85 \sim 198] \times [512] \times [512]$ pixels in dimensions $D \times H \times W$, where D represents the depth, H is the height, and W is the width. As the BTCV dataset is used for out-of-distribution performance evaluation, all its data are used for testing. The in-plane pixel spacing in this dataset varies between 0.59mm to 0.98mm, and the slice thickness ranges from 2.50mm to 5.00mm. The dataset provides pixel-wise annotations for 14 classes: spleen, right kidney, left kidney, gall bladder, esophagus, liver, stomach, aorta, postcava, portal vein and splenic vein, pancreas, right adrenal gland, left adrenal gland, and duodenum.

LiTS ([2017](#)) ([Bilic et al., 2023](#)) comprises 131 scans with volume size range from $[74 \sim 987] \times [512] \times [512]$ pixels in dimensions $D \times H \times W$. Out of the 131 scans, 95 are used for training, 16 for validation, and 20 for testing. The in-plane pixel spacing in this dataset varies between 0.56mm and 1.00mm, and the slice thickness ranges from 0.70mm to 5.00mm. The dataset provides annotations for 2 classes: liver and liver tumor.

KiTS ([Heller et al., 2019](#)) comprises 210 scans with volume sizes ranging from $[29 \sim 1059] \times [512] \times [512, 796]$ pixels in dimensions $D \times H \times W$. Out of the 210 scans, 142 are used for training, 22 for validation, and 46 for testing. The in-plane pixel spacing in this dataset varies between 0.44mm and 1.04mm, and the slice thickness ranges from 0.50mm to 5.00mm. The dataset provides annotations for 4 classes: left kidney, right kidney, kidney tumor, and kidney crystal.

MSD - Spleen ([Antonelli et al., 2022](#)) comprises 41 scans with volume size range from $[31 \sim 168] \times [512] \times [512]$ pixels in dimensions $D \times H \times W$. Out of the 41 scans, 27 are used for training, 4 for validation, and 10 for testing. The in-plane pixel spacing in this dataset varies between 0.61mm and 0.98mm, and the slice thickness ranges from 1.50mm to 8.00mm. The dataset provides annotations for 1 class: spleen.

MSD - Pancreas ([Antonelli et al., 2022](#)) comprises 281 scans with volume size range from $[37 \sim 751] \times [512] \times [512]$ pixels in dimensions $D \times H \times W$. Out of the 281 scans, 198 are used for training, 29 for validation, and 54 for testing. The in-plane pixel spacing in this dataset varies between 0.54mm and 0.98mm, and the slice thickness ranges from 0.63mm to 7.50mm. The dataset provides annotations for 2 classes: pancreas and pancreas tumor.

Table A.3: This table presents the dataset information used in the paper. To simulate real-world conditions, each dataset is treated as an individual client, with all available class annotations utilized. Consequently, class distributions may vary between clients, and some classes may overlap across different clients, mirroring real-world scenarios.

Datasets	# Labels	# Train Imgs	Annotated Structures
LiTS	2	131	Liver, Liver Tumor
KiTS	4	210	Left Kidney (LKid), Right Kidney (RKid), Kidney Tumor, Kidney Crystal
MSD-Spleen	1	41	Spleen
MSD-Pancreas	2	281	Pancreas, Pancreas Tumor
AMOS22	15	200	Spleen, RKid, LKid, Gall bladder (Gall), Esophagus, Liver, Stomach, Aorta, IVC, Pancreas, Right adrenal gland (RAG), Left adrenal gland (LAG), Duodenum, Bladder, Prostate
BTCV	14	30	Spleen, RKid, LKid, Gall, Esophagus, Liver, Stomach, Aorta, IVC, R&S Veins, Pancreas, RAG, LAG, Duodenum

AMOS ([Ji et al., 2022](#)) comprises 200 scans with volume size range from $[64 \sim 512] \times [60 \sim 768] \times [192 \sim 768]$ pixels in dimensions $D \times H \times W$. Out of the 200 scans, 145 are used for training, 23 for validation, and 32 for testing. The in-plane pixel spacing in this dataset varies between 0.45mm and 3.00mm, and the slice thickness ranges from 0.82mm to 5.00mm. The dataset provides annotations for 15 classes: spleen, right kidney, left kidney, gall bladder, esophagus, liver, stomach, aorta, postcava, pancreas, right adrenal gland, left adrenal gland, duodenum, bladder, and prostate.

References

Afonin, A., Karimireddy, S.P., 2021. Towards model agnostic federated learning using knowledge distillation. arXiv preprint arXiv:2110.15210 .

Antonelli, M., Reinke, A., Bakas, S., Farahani, K., Kopp-Schneider, A., Landman, B.A., Litjens, G., Menze, B., Ronneberger, O., Summers, R.M., et al., 2022. The medical segmentation decathlon. *Nature communications* 13, 4128.

Babakniya, S., Fabian, Z., He, C., Soltanolkotabi, M., Avestimehr, S., 2024. A data-free approach to mitigate catastrophic forgetting in federated class incremental learning for vision tasks. *Advances in Neural Information Processing Systems* 36.

Bilic, P., Christ, P., Li, H.B., Vorontsov, E., Ben-Cohen, A., Kaassis, G., Szeskin, A., Jacobs, C., Mamani, G.E.H., Chartrand, G., et al., 2023. The liver tumor segmentation benchmark (lits). *Medical Image Analysis* 84, 102680.

Chen, Z., Yang, H., Quek, T., Chong, K.F.E., 2023. Spectral co-distillation for personalized federated learning. *Advances in Neural Information Processing Systems* 36, 8757–8773.

Ciçek, Ö., Abdulkadir, A., Lienkamp, S.S., Brox, T., Ronneberger, O., 2016. 3d u-net: learning dense volumetric segmentation from sparse annotation, in: *Medical Image Computing and Computer-Assisted Intervention—MICCAI 2016: 19th International Conference, Athens, Greece, October 17–21, 2016, Proceedings, Part II* 19, Springer. pp. 424–432.

Dong, J., Wang, L., Fang, Z., Sun, G., Xu, S., Wang, X., Zhu, Q., 2022. Federated class-incremental learning, in: *Proceedings of the IEEE/CVF conference on computer vision and pattern recognition*, pp. 10164–10173.

Gong, X., Sharma, A., Karanam, S., Wu, Z., Chen, T., Doermann, D., Innanje, A., 2021. Ensemble attention distillation for privacy-preserving federated learning, in: *Proceedings of the IEEE/CVF International Conference on Computer Vision*, pp. 15076–15086.

Hatamizadeh, A., Nath, V., Tang, Y., Yang, D., Roth, H.R., Xu, D., 2021. Swin unetr: Swin transformers for semantic segmentation of brain tumors in mri images, in: *International MICCAI brainlesion workshop*, Springer. pp. 272–284.

He, C., Annavaram, M., Avestimehr, S., 2020. Group knowledge transfer: Federated learning of large cnns at the edge. *Advances in Neural Information Processing Systems* 33, 14068–14080.

Heller, N., Sathianathan, N., Kalapara, A., Walczak, E., Moore, K., Kaluzniak, H., Rosenberg, J., Blake, P., Rengel, Z., Oestreich, M., et al., 2019. The kits19 challenge data: 300 kidney tumor cases with clinical context, ct semantic segmentations, and surgical outcomes. arXiv preprint arXiv:1904.00445 .

Hinton, G., 2015. Distilling the knowledge in a neural network. arXiv preprint arXiv:1503.02531 .

Jeong, E., Oh, S., Kim, H., Park, J., Bennis, M., Kim, S.L., 2018. Communication-efficient on-device machine learning: Federated distillation and augmentation under non-iid private data. arXiv preprint arXiv:1811.11479 .

Ji, Y., Bai, H., Ge, C., Yang, J., Zhu, Y., Zhang, R., Li, Z., Zhanng, L., Ma, W., Wan, X., et al., 2022. Amos: A large-scale abdominal multi-organ benchmark for versatile medical image segmentation. *Advances in neural information processing systems* 35, 36722–36732.

Kim, S., Park, H., Kang, M., Jin, K.H., Adeli, E., Pohl, K.M., Park, S.H., 2024. Federated learning with knowledge distillation for multi-organ segmentation with partially labeled datasets. *Medical Image Analysis* 95, 103156.

Landman, B., Xu, Z., Iglesias, J., Styner, M., Langerak, T., Klein, A., 2015. Miccai multi-atlas labeling beyond the cranial vault—workshop and challenge, in: *Proc. MICCAI Multi-Atlas Labeling Beyond Cranial Vault—Workshop Challenge*, p. 12.

Li, Y., Li, Q., Wang, H., Li, R., Zhong, W., Zhang, G., 2024. Towards efficient replay in federated incremental learning, in: *Proceedings of the IEEE/CVF Conference on Computer Vision and Pattern Recognition*, pp. 12820–12829.

Lin, T., Kong, L., Stich, S.U., Jaggi, M., 2020. Ensemble distillation for robust model fusion in federated learning. *Advances in neural information processing systems* 33, 2351–2363.

Liu, J., Zhang, Y., Chen, J.N., Xiao, J., Lu, Y., A Landman, B., Yuan, Y., Yuille, A., Tang, Y., Zhou, Z., 2023. Clip-driven universal model for organ segmentation and tumor detection, in: *Proceedings of the IEEE/CVF International Conference on Computer Vision*, pp. 21152–21164.

Liu, Q., Chen, C., Qin, J., Dou, Q., Heng, P.A., 2021. Feddg: Federated domain generalization on medical image segmentation via episodic learning in continuous frequency space, in: *Proceedings of the IEEE/CVF conference on computer vision and pattern recognition*, pp. 1013–1023.

Luo, X., Liao, W., Xiao, J., Chen, J., Song, T., Zhang, X., Li, K., Metaxas, D.N., Wang, G., Zhang, S., 2021. Word: A large scale dataset, benchmark and clinical applicable study for abdominal organ segmentation from ct image. arXiv preprint arXiv:2111.02403 .

Ma, Y., Xie, Z., Wang, J., Chen, K., Shou, L., 2022. Continual federated learning based on knowledge distillation., in: *IJCAI*, pp. 2182–2188.

McMahan, B., Moore, E., Ramage, D., Hampson, S., y Arcas, B.A., 2017. Communication-efficient learning of deep networks from decentralized data, in: *Artificial intelligence and statistics*, PMLR. pp. 1273–1282.

Mora, A., Tenison, I., Bellavista, P., Rish, I., 2024. Knowledge distillation in federated learning: a practical guide, in: Proceedings of the Thirty-Third International Joint Conference on Artificial Intelligence, pp. 8188–8196.

Qi, D., Zhao, H., Li, S., 2023. Better generative replay for continual federated learning. arXiv preprint arXiv:2302.13001 .

Radford, A., Kim, J.W., Hallacy, C., Ramesh, A., Goh, G., Agarwal, S., Sastry, G., Askell, A., Mishkin, P., Clark, J., et al., 2021. Learning transferable visual models from natural language supervision, in: International conference on machine learning, PMLR. pp. 8748–8763.

Sattler, F., Marban, A., Rischke, R., Samek, W., 2021. Cfd: Communication-efficient federated distillation via soft-label quantization and delta coding. IEEE Transactions on Network Science and Engineering 9, 2025–2038.

Shen, C., Xue, M., Wang, X., Song, J., Sun, L., Song, M., 2019. Customizing student networks from heterogeneous teachers via adaptive knowledge amalgamation, in: Proceedings of the IEEE/CVF International Conference on Computer Vision, pp. 3504–3513.

Tran, M.T., Le, T., Le, X.M., Harandi, M., Phung, D., 2024. Text-enhanced data-free approach for federated class-incremental learning, in: Proceedings of the IEEE/CVF Conference on Computer Vision and Pattern Recognition, pp. 23870–23880.

Usmanova, A., Portet, F., Lalande, P., Vega, G., 2021. A distillation-based approach integrating continual learning and federated learning for pervasive services. arXiv preprint arXiv:2109.04197 .

Wang, J., Jin, Y., Stoyanov, D., Wang, L., 2023. Feddp: Dual personalization in federated medical image segmentation. IEEE Transactions on Medical Imaging .

Wang, J., Jin, Y., Wang, L., 2022. Personalizing federated medical image segmentation via local calibration, in: European Conference on Computer Vision, Springer. pp. 456–472.

Wicaksana, J., Yan, Z., Zhang, D., Huang, X., Wu, H., Yang, X., Cheng, K.T., 2022. Fedmix: Mixed supervised federated learning for medical image segmentation. IEEE Transactions on Medical Imaging 42, 1955–1968.

Wu, N., Sun, Z., Yan, Z., Yu, L., 2024. Feda3i: Annotation quality-aware aggregation for federated medical image segmentation against heterogeneous annotation noise, in: Proceedings of the AAAI Conference on Artificial Intelligence, pp. 15943–15951.

Xu, A., Li, W., Guo, P., Yang, D., Roth, H.R., Hatamizadeh, A., Zhao, C., Xu, D., Huang, H., Xu, Z., 2022. Closing the generalization gap of cross-silo federated medical image segmentation, in: Proceedings of the IEEE/CVF Conference on Computer Vision and Pattern Recognition, pp. 20866–20875.

Xu, X., Deng, H.H., Gateno, J., Yan, P., 2023. Federated multi-organ segmentation with inconsistent labels. IEEE transactions on medical imaging 42, 2948–2960.

Zhang, J., Chen, C., Zhuang, W., Lyu, L., 2023. Target: Federated class-continual learning via exemplar-free distillation, in: Proceedings of the IEEE/CVF International Conference on Computer Vision, pp. 4782–4793.

Zhu, M., Chen, Z., Yuan, Y., 2023. Feddm: Federated weakly supervised segmentation via annotation calibration and gradient de-conflicting. IEEE Transactions on Medical Imaging 42, 1632–1643.